eppendorf

The Smarter Solution

Flexible, powerful, industrial

Many engineering parameters need to be considered to establish a successful mAbs process. The BioFlo® 320 offers a wide range of options to meet your needs. It combines industrial design, flexibility between interchangeable autoclavable and single-use bioreactors, and universal gas control strategy for your applications.

> **New Scale Up Assist** software: Fast and easy calculation of important process parameter based on P/V or constant tip speed
> Compatible with the BioBLU® Single-use Bioreactor portfolio
> **Scalable:** Extensive working volume range of 250 mL – 40 L
> **Efficient:** Multi-unit control of up to eight systems from a single interface

www.eppendorf.com/BioFlo320

Received: 26 March 2021 | Revised: 9 June 2021 | Accepted: 19 June 2021

DOI: 10.1002/bit.27868

ARTICLE

BIOTECHNOLOGY AND BIOENGINEERING WILEY

Process development for cross-flow diafiltration-based VLP disassembly: A novel high-throughput screening approach

Nils Hillebrandt | Philipp Vormittag | Annabelle Dietrich | Christina H. Wegner | Jürgen Hubbuch

Institute of Engineering in Life Sciences - Section IV: Biomolecular Separation Engineering, Karlsruhe Institute of Technology (KIT), Karlsruhe, Baden-Württemberg, Germany

Correspondence
Jürgen Hubbuch, Institute of Engineering in Life Sciences - Section IV: Biomolecular Separation Engineering, Karlsruhe Institute of Technology (KIT), Fritz-Haber-Weg 2, 76131 Karlsruhe, Baden-Württemberg, Germany.
Email: juergen.hubbuch@kit.edu

Funding information
Deutsche Forschungsgemeinschaft, Grant/Award Number: 273937032 (SPP 1934)

Abstract

Virus-like particles (VLPs) are particulate structures, which are applied as vaccines or delivery vehicles. VLPs assemble from subunits, named capsomeres, composed of recombinantly expressed viral structural proteins. During downstream processing, *in vivo*-assembled VLPs are typically dis- and reassembled to remove encapsulated impurities and to improve particle morphology. Disassembly is achieved in a high-pH solution and by the addition of a denaturant or reducing agent. The optimal disassembly conditions depend on the VLP amino acid sequence and structure, thus requiring material-consuming disassembly experiments. To this end, we developed a low-volume and high-resolution disassembly screening that provides time-resolved insight into the VLP disassembly progress. In this study, two variants of C-terminally truncated hepatitis B core antigen were investigated showing different disassembly behaviors. For both VLPs, the best capsomere yield was achieved at moderately high urea concentration and pH. Nonetheless, their disassembly behaviors differed particularly with respect to disassembly rate and aggregation. Based on the high-throughput screening results, a diafiltration-based disassembly process step was developed. Compared with mixing-based disassembly, it resulted in higher yields of up to 0.84 and allowed for integrated purification. This process step was embedded in a filtration-based process sequence of disassembly, capsomere separation, and reassembly, considerably reducing high-molecular-weight species.

KEYWORDS
cross-flow filtration, disassembly, downstream processing, high-throughput screening, virus-like particles

1 | INTRODUCTION

Virus-like particles (VLPs) are multimolecule structures that resemble the native virus they were derived from, but lack infectious nucleic acids (Chackerian, 2007). Their particulate and repetitive structure makes them highly immunogenic, which has been harnessed by several licensed vaccines, such as VLPs against hepatitis B virus and human papillomavirus infection (Bryan et al., 2016; McAleer et al., 1984). Chimeric VLPs are VLPs which incorporate a foreign antigenic epitope against which an immune reaction is intended. This has been evaluated in several

preclinical and clinical trials, and recently, a vaccine against the circumsporozoite protein of the malaria pathogen has been locally approved (European Medicines Agency, 2015). Recent efforts to develop VLP-based severe acute respiratory syndrome coronavirus 2 (SARS-CoV-2) vaccines underline the flexibility and simplicity of chimeric VLPs (Ghorbani et al., 2020; Yang et al., 2021). However, the versatile platform of chimeric VLPs not only comes with promises, but also with fundamental challenges, such as the ability to form stable capsids (Borisova et al., 1999; Böttcher et al., 2006; Nassal et al., 2005; Pumpens & Grens, 2001). Challenges related to the production process include the limited solubility of candidate molecules (Jegerlehner, 2002; Karpenko et al., 2000; Vormittag et al., 2020a) and the dependence of process parameters on molecular properties, which are both influenced by the amino acid sequence of the inserted foreign antigenic epitope (Rüdt et al., 2019). A typical production process is shown in Figure 1a. Process steps that are influenced by the epitope insertion are, for example, precipitation, where a varying amount of ammonium sulfate is required for VLP precipitation (Hillebrandt et al., 2020; Vormittag et al., 2020b), and VLP reassembly, which has been proposed to depend on VLP zeta potential (Rüdt et al., 2019). VLPs are disassembled (dissociated into capsomeres) and reassembled (capsomeres triggered to form capsids) to improve structural homogeneity, stability, and immunogenicity (Zhao, Allen, et al., 2012; Zhao, Modis, et al., 2012). Disassembly is realized by a high pH and low ionic strength, often adding denaturants or reducing agents (Bin Mohamed Suffian et al., 2017; Mach et al., 2006; McCarthy et al., 1998; Singh & Zlotnick, 2003; Strods et al., 2015; Zhang et al., 2021), while reassembly is achieved at neutral pH and high ionic strength (Mach et al., 2006; Zlotnick et al., 1996). As disassembly releases capsid-internal impurities and typically leads to incomplete disassembly or aggregate formation, a capsomere separation step is added between dis- and

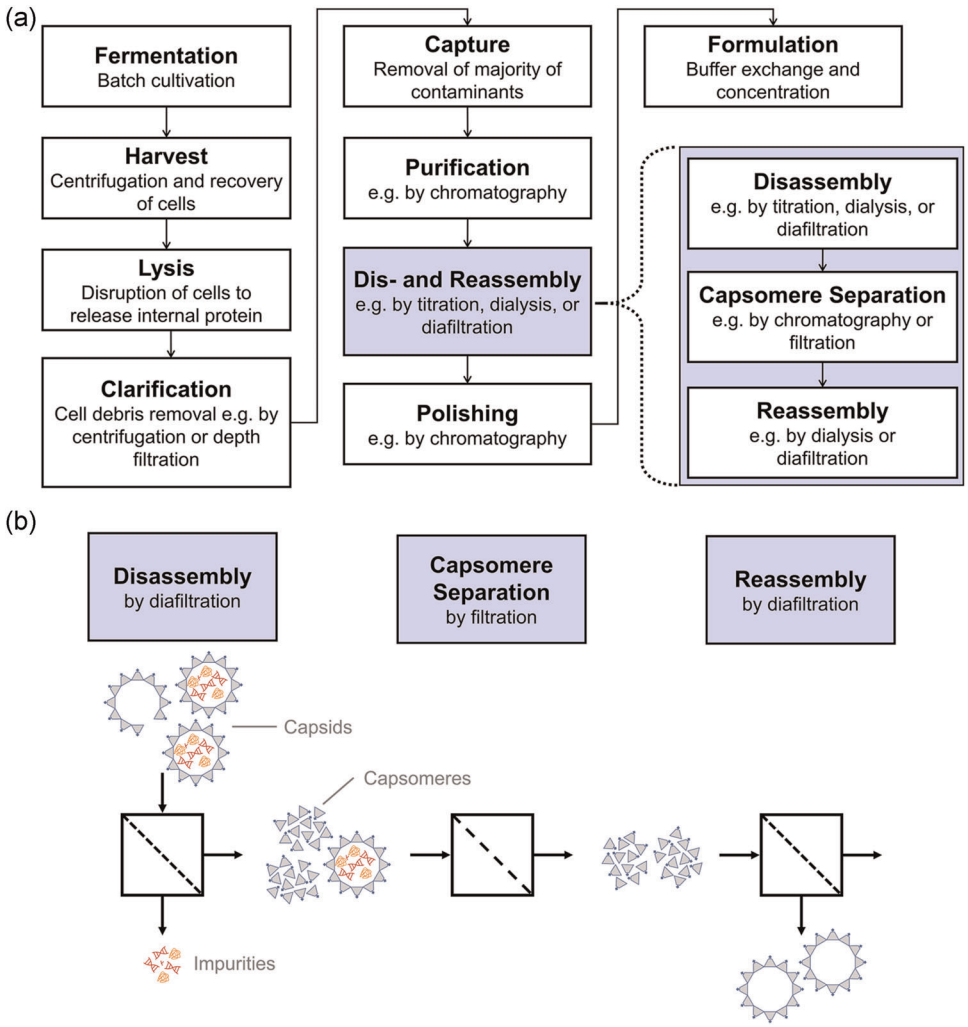

FIGURE 1 (a) Process of intracellularly produced, *in vivo*-assembled capsids, highlighting unique virus-like particle (VLP) process steps. Compared with other biotechnological products, upstream processing and primary purification are followed by a sequence of disassembly, capsomere separation, and reassembly. This sequence allows for the improvement of particle homogeneity and removal of encapsulated impurities. (b) Concept of a filtration-based VLP purification cascade. Capsids are disassembled by cross-flow diafiltration (DF) into a disassembly buffer while the capsomeres are retained by the membrane. Encapsulated impurities are released during disassembly and washed out if smaller than the membrane molecular weight cut-off. Non-disassembled capsids and potential aggregates are separated by a dead-end ultrafiltration step. The capsids are then reassembled in a second cross-flow DF step into a DF buffer that favors the assembled state [Color figure can be viewed at wileyonlinelibrary.com]

reassembly (Zlotnick et al., 1996). As a denaturant, urea has been investigated at several concentrations for hepatitis B core antigen (HBcAg) VLP disassembly into HBcAg dimers (capsomeres) (Singh & Zlotnick, 2003; Zhang et al., 2021), further referred to as dimers. These publications show that an increasing urea concentration leads to a more complete and rapid disassembly, while urea concentrations of ≥4 M resulted in protein denaturation, which, in turn, can lead to aggregation or the inability to reassemble. It, therefore, seems reasonable to use urea concentrations for disassembly which are high enough to maximize the dimer yield but do not result in protein denaturation. For chimeric VLPs, it is conceivable that the inserted epitope influences the optimal disassembly solution conditions. Unpublished results on chimeric HBcAg disassembly by our laboratory confirm these assumptions.

VLP disassembly is typically achieved by the addition of disassembly agents (Mach et al., 2006; McCarthy et al., 1998; Singh & Zlotnick, 2003; Zlotnick et al., 1996), mixing VLP product with a disassembly buffer (Bin Mohamed Suffian et al., 2017; Lee & Tan, 2008; Liew et al., 2012; Zhang et al., 2021), or by dialysis (Holmes et al., 2015; Strods et al., 2015). While mixing is fast, it leads to dilution. Dialysis does not significantly change the original concentration and has the capability to remove some of the (encapsulated) impurities through the dialysis membrane (Mach et al., 2006) but is a slow process (Phillips & Signs, 2004). In recent publications, we have demonstrated the utility of transferring VLP process steps, namely capture and VLP reassembly, to a cross-flow filtration (CFF) unit (Hillebrandt et al., 2020; Rüdt et al., 2019). Figure 1a shows that these two process steps frame the disassembly step, which is one of the reasons why it was presumed to be useful to transfer this process step to cross-flow diafiltration (DF). As CFF process development is time- and material-consuming, it can be accelerated if the optimal DF buffer composition is known before.

In this study, we developed a time-resolved high-throughput disassembly screening for (chimeric) VLP candidates. This approach aims to reduce the experimental effort to identify optimal disassembly conditions for different VLPs and for CFF process development. As candidate VLP material is scarce at an early stage of process development, it is highly desirable to develop a screening method which requires a small amount of VLPs. To this end, we developed a low-volume, fast, and accurate screening method that allows for the assessment of VLP dimer yield and kinetic data based on a high-performance liquid chromatography (HPLC) system. Disassembly of a C-terminally truncated HBcAg and a chimeric C-terminally truncated HBcAg VLP with a polyhistidine tag was investigated (referred to as Cp149 and VLP A, respectively). Optimal disassembly conditions were selected for DF process development. This integrated DF process step allows for disassembly and depletion of impurities simultaneously. Additionally, we show that the developed disassembly process step can be integrated into a filtration-based sequence of disassembly, dimer separation, and reassembly (Figure 1b). The results presented in this study underline the influence of inserted peptides on the optimal conditions for disassembly and demonstrate the usefulness of the developed high-throughput screening method and its transferability to a filtration-based process.

2 | MATERIALS AND METHODS

2.1 | Materials, buffers, and VLPs

All chemicals were purchased from Merck KGaA, unless otherwise stated. Solutions and buffers were prepared with ultrapure water (PURELAB Ultra; ELGA LabWater). All buffers were pH-adjusted with 32% HCl or 4 M NaOH using a SenTix62 pH electrode (WTW) at a HI 3220 pH meter (Hanna Instruments). Solutions were filtered before use and analysis through 0.2 µm cellulose acetate (VWR) or Millex-GV 0.22 µm polyvinylidene fluoride filters (Merck Millipore), often with glass fiber pre-filtration (Minisart GF; Sartorius Stedim Biotech GmbH). The plasmid for Cp149, a C-terminally truncated HBcAg protein (amino acids 1 to149 (Zlotnick et al., 1996)), was generously provided by Prof. Adam Zlotnick (Indiana University). BioNTech Protein Therapeutics GmbH generously provided the chimeric HBcAg VLP A plasmid. VLP A was C-terminally truncated, contained an inserted epitope, and incorporated a C-terminal polyhistidine tag, similar as in (Schumacher et al., 2018). The Cp149 and VLP A protein dimers had a molecular weight of approximately 34 and 40 kDa, respectively. The 280 nm extinction coefficients were derived from the web-tool ProtParam (Gasteiger et al., 2005) and were 1.764 $L \cdot g^{-1} \cdot cm^{-1}$ for Cp149 and 1.558 $L \cdot g^{-1} \cdot cm^{-1}$ for VLP A. Concentrations were calculated using Beer's law and the 280 nm absorbance peak area derived from size-exclusion chromatography (SEC) HPLC. The HBcAg concentration of the VLP feedstock was determined analogously using the total 280 nm absorbance and a NanoDrop 2000c spectrometer (Thermo Fisher Scientific). HBcAg was expressed in *Escherichia coli*, liberated by lysis, precipitated and re-dissolved applying a centrifugation protocol similarly as described in a recent article (Hillebrandt et al., 2020). Additionally, the re-dissolved and sterile-filtered VLP solution was purified by DF and multimodal SEC as described in the Supporting Information Section S1.

2.2 | Disassembly buffer compositions

The disassembly time series (DisA-TS) is a two-step procedure and described in detail in Section 2.3. Briefly, a batch disassembly reaction is followed by SEC-HPLC analysis under the same liquid phase conditions as in the batch reaction. This batch reaction is initiated by mixing equal volumes of HBcAg VLP solution and disassembly buffer to reach the target disassembly conditions after mixing. For all conditions, the common target concentrations were 50 mM Tris and 1 $g \cdot L^{-1}$ HBcAg. Urea concentrations (c_{urea}) and pH were screened in the ranges from 0 to 4 M and pH 7.2 to 9.0, respectively. The selection of the condition ranges was based on unpublished pre-experiments and other publications investigating HBcAg VLPs (Schumacher et al., 2018; Singh & Zlotnick, 2003). Each target condition required a distinct composition of the added disassembly buffer which was composed of Tris, urea, and titrant. Therefore, the required titrant concentration ($c_{titrant}$) of each disassembly buffer was determined to eventually reach the target pH after mixing with VLP solution. The procedure of this disassembly buffer composition determination is explained in Figure 2a. It was assumed that the protein

buffer capacity of HBcAg at a concentration of 1 g·L^{-1} is negligible. Under this assumption, 50 mM Tris at pH 7.2 was used to mimic the VLP solution and thereby minimize the VLP (product) consumption. The experiments were performed in duplicates and at a 200 mL scale to minimize pipetting errors. The results were exemplarily confirmed by mixing VLP solution and disassembly buffer at a 200 µL scale and measuring the resulting pH using an Orion PerpHecT ROSS combination microelectrode (Thermo Fisher Scientific).

2.3 | DisA-TS and disassembly on column (DisA-OC)

The DisA-TS is a hybrid disassembly screening in nature. It consists of a batch disassembly reaction followed by SEC-HPLC analyses. During the latter, the disassembly reaction continues until detection, similar to the on-column disassembly reaction described below. The time series was started at time t_0 by adding 250 µL disassembly buffer to 250 µL VLP solution in a 2.2 mL deep-well plate (VWR) in intervals of 7.5 min between each well. The mixtures were incubated at 23°C and repeatedly analyzed by SEC-HPLC over a period of 24 h at times t_i (Figure 2b). Analytical SEC was performed with 20 µL injections on an AdvanceBio SEC 300 Å, 4.6 × 150 mm, 2.7 µm column (Agilent Technologies) at a Dionex Ultimate 3000 RS UHPLC system with a diode array detector controlled by Chromeleon version 6.8 SR15 (Thermo Fisher Scientific). The mobile phase was adapted to the sample's target disassembly condition, and a flow rate of 0.35 mL·min^{-1} was applied. Samples at pH 9.0 were analyzed at pH 8.0 due to the limited pH compatibility of the column. The efficiency of a disassembly condition was described by the (total) dimer yield

$$Y_{\mathrm{dimer,tot}} = \frac{c_{\mathrm{dimer,tot}}(t)}{\bar{c}_{\mathrm{VLP}}(t_0) + \bar{c}_{\mathrm{dimer}}(t_0)}, \quad (1)$$

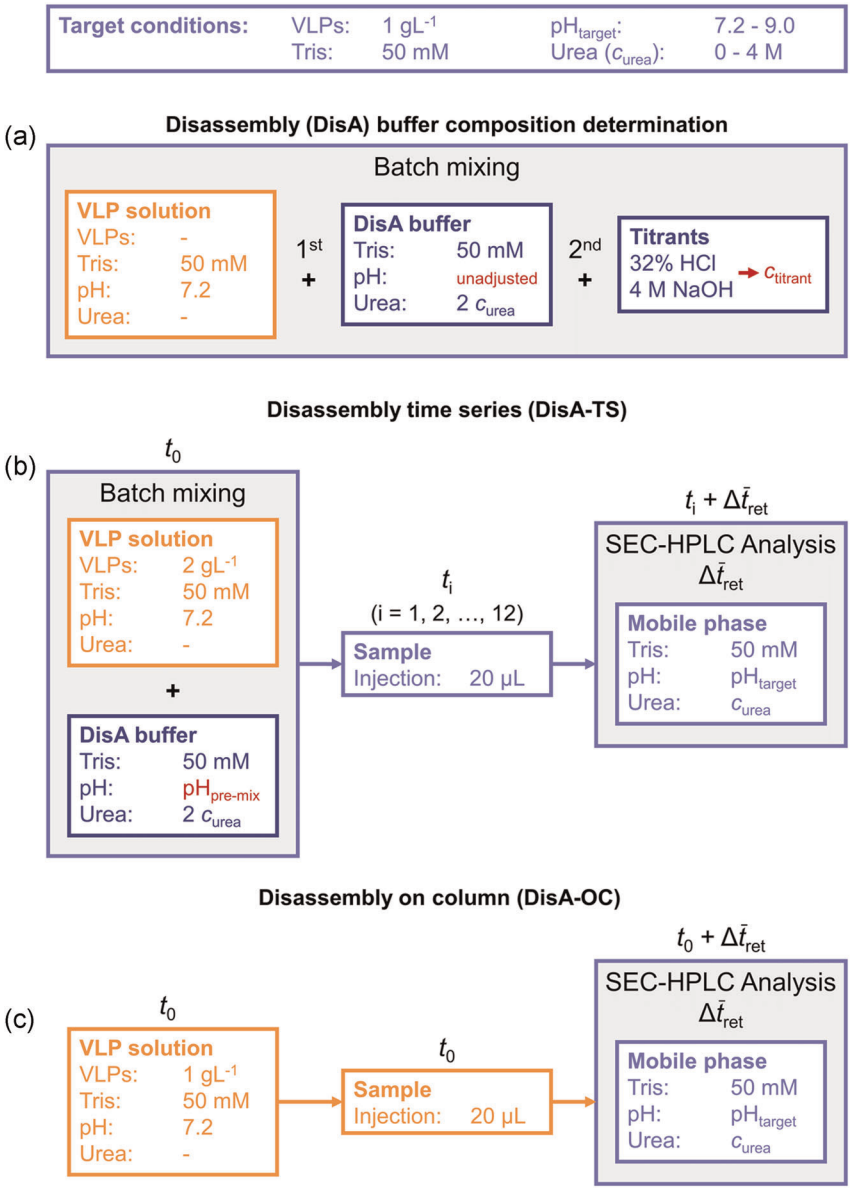

FIGURE 2 Schematic of the developed screening procedures. The large gray boxes represent mixtures of solutions represented by smaller boxes. (a) A separate experiment is required to determine each disassembly buffer composition by titration. First, VLP solution[a] is mixed with pH-unadjusted (non-titrated) disassembly buffer. Second, the mixture is titrated to the target pH (pH_{target}) and the required amount of titrant (either NaOH or HCl) is used to determine the titrant concentration of the final disassembly buffer $c_{titrant}$. (b) The DisA-TS is started at time t_0 by mixing VLP solution with an equal volume of disassembly buffer to achieve the target disassembly condition. Samples are repeatedly drawn at times t_i (i = 1, 2, ...,12) and analyzed by SEC-HPLC. The obtained results are assigned to $t = t_i + \Delta\bar{t}_{ret}$, where $\bar{t}_{ret}$ is the average SEC-HPLC retention time of the dimer peak. (c) The DisA-OC is started by injecting VLP solution onto the SEC-HPLC column under disassembly conditions at time t_0 without prior mixing or pre-experiments. The obtained SEC-HPLC results are assigned to $t = t_0 + \Delta\bar{t}_{ret}$. [a]At low target HBcAg concentrations of up to approximately 1 g·L^{-1}, the protein buffer capacity is negligible. Therefore, the determination of the disassembly buffer composition can be performed with VLP solution with zero HBcAg concentration, i.e. 50 mM Tris, pH 7.2 buffer. c, concentration; DisA-OC, disassembly on column; DisA-TS, disassembly time series; HBcAg, hepatitis B core antigen; HPLC, high-performance liquid chromatography; SEC, size-exclusion chromatography; VLP, virus-like particle; t, point in time [Color figure can be viewed at wileyonlinelibrary.com]

where $c_{\mathrm{dimer,tot}}(t)$ is the total dimer concentration at the time t after start of the disassembly at t_0. Furthermore, $\bar{c}_{\mathrm{VLP}}(t_0)$ and $\bar{c}_{\mathrm{dimer}}(t_0)$ are the mean initial concentrations of HBcAg VLPs and dimers, respectively, which are present in the VLP feedstock prior to the disassembly reaction. Mean concentrations from 28 samples of the VLP solution at 1 g·L^{-1} HBcAg were determined by SEC-HPLC as described above but with 50 mM Tris at pH 7.2 as mobile phase. During the 24 h DisA-TS, evaporation was observed. To estimate an average volumetric evaporation rate, the total HBcAg concentration of a VLP solution was analyzed twice with an interval of 20 h. The mean evaporation rate was then converted into evaporation correction factors $f_v(t)$ that enabled the calculation of an evaporation-corrected concentration

$$c_{\mathrm{dimer,tot}}(t) = \frac{\tilde{c}_{\mathrm{dimer,tot}}(t)}{f_v(t)}, \tag{2}$$

where $\tilde{c}_{\mathrm{dimer,tot}}(t)$ is the measured concentration during the DisA-TS. A derivation of $f_v(t)$ and Equation (2) can be found in Appendix A.

To investigate the disassembly reaction with a shorter time interval and without prior mixing or batch disassembly, the above-mentioned SEC-HPLC method was used as an additional screening tool. This approach is in the following referred to as DisA-OC and shown in Figure 2c. To this end, a VLP solution with 1 g·L^{-1} HBcAg (50 mM Tris, pH 7.2) was analyzed by SEC-HPLC applying the same flow rate and mobile phases at target disassembly conditions as described above. For our SEC-HPLC setup, we determined the observed time interval $\Delta\bar{t}_{\mathrm{ret}} = \bar{t}_{\mathrm{ret}} - t_{\mathrm{inj}} = 3.36$ min, where $\bar{t}_{\mathrm{ret}}$ is the average retention time of the dimer peak over all experiments and t_{inj} is the injection time. For DisA-OC, the start of the disassembly was defined as $t_0 = t_{\mathrm{inj}}$.

The disassembly rate k_0 was calculated by

$$k_0 = \frac{c_{\mathrm{dimer,tot}}(t) - \bar{c}_{\mathrm{dimer}}(t_0)}{t - t_0}. \tag{3}$$

In the following, we define $k_{0,\mathrm{DisA\text{-}TS}}$ as the rate obtained by DisA-TS at $t = t_1 + \Delta\bar{t}_{\mathrm{ret}}$ and $k_{0,\mathrm{DisA\text{-}OC}}$ as the rate obtained by DisA-OC at $t = t_0 + \Delta\bar{t}_{\mathrm{ret}}$, where t_1 is the time of the first sampling after approximately 30 min.

2.4 | Filtration-based disassembly, dimer separation, and reassembly

The sequential process of disassembly, dimer separation, and reassembly was realized in three steps as shown in Figure 1b. Step (I) was DF-based disassembly into a disassembly buffer using a 10 kDa molecular weight cut-off (MWCO), 88 cm^2 Ultracel Pellicon 3 membrane (Merck Millipore) followed by an 18 h overnight hold at 5°C and subsequently by filtration through a 0.2 µm pore size cellulose acetate syringe filter (VWR). Note, that urea concentration and pH of the DF disassembly buffer were at target disassembly conditions. Step (II) consisted of dimer separation by dead-end ultrafiltration using Vivaspin Turbo 15 RC centrifugal filters with 100 kDa MWCO regenerated cellulose membranes (Sartorius Stedim Biotech GmbH). The disassembly solution was split into six centrifugal filters, which were operated at a relative centrifugal force of 1000 for 15 min, and the product was collected in the filtrate/permeate. The remaining retentate was equally reprocessed with a new filter. Step (III) was DF-based reassembly into 50 mM Tris buffer at pH 7.2 with 650 mM NaCl using a 10 kDa MWCO, 200 cm^2 Sartocon Slice 200 (Sartorius Stedim Biotech GmbH) where the product was collected from the retentate. Both DF process steps were realized on a KrosFlo Research KRIIi CFF system (Spectrum Labs) at a constant volume of 30 mL, a feed flow rate of 30 mL·min^{-1}, and permeate flow rate control at 2 mL·min^{-1} as implemented previously (Hillebrandt et al., 2020). The corresponding permeate flux setpoints were 13.6 and 6.0 L·m^{-2}·h^{-1} for disassembly and reassembly, respectively. The whole process was performed at room temperature (22.5 ± 0.5°C), unless otherwise stated.

At-line analysis of DF-based disassembly was performed analogously to the HPLC method in the DisA-TS. The mobile phase composition was adapted to the current theoretical buffer composition in the retentate. This was realized by mixing (A) 50 mM Tris at pH 7.2 with (B) the DF disassembly buffer. Assuming ideal mixing and unrestricted permeability of urea during DF, the fraction of (B) equals $1 - e^{-\mathrm{DV}}$, where DV represents exchanged DF volumes (Kurnik et al., 1995). Feed and reassembly samples were analyzed with a Bio SEC-5 1000 Å, 4.6 × 300 mm, 5 µm column (Agilent Technologies), at a flow rate of 0.4 mL·min^{-1}, and in 50 mM Tris at pH 7.2 as mobile phase. Dimer separation samples were analyzed using the same column with the DF disassembly buffer as mobile phase. The resulting dimer concentrations before and after dimer separation were used to calculate the apparent retention coefficient of dimers under process conditions as

$$R_{\mathrm{dimer}} = 1 - \frac{c_{\mathrm{dimer,Sep}}}{c_{\mathrm{dimer,DisA}}}. \tag{4}$$

The dimer concentrations after disassembly/hold ($c_{\mathrm{dimer,DisA}}$) and after dimer separation ($c_{\mathrm{dimer,Sep}}$) represent the bulk (feed) and permeate concentrations, respectively.

3 | RESULTS AND DISCUSSION

DisA-Ts: The long-term development of the disassembly reaction was monitored using an initial batch disassembly reaction followed by 12 SEC-HPLC analyses over a time period of 24 h. The time series was initiated by mixing equal volumes of VLP solution and disassembly buffer (Figure 2b). The ionic strength of this mixture is different from the ones of the individual solutions before mixing. The ionic strength of a solution influences the pK_a of weak acids/bases, such as Tris, and ultimately the solution pH (Beynon & Easterby, 1996). Therefore, the pH does not change linearly with the volume shares upon mixing of VLP solution and disassembly buffer. This nonlinear behavior is not expected for non-dissociating species, such as urea in this screening. Next to the ionic strength, the urea concentration influences the pH of aqueous solutions (Bull et al., 1964). Instead of correcting the pH of the mixture by titration,

the exact amount of titrant was determined beforehand in a separate experiment (Figure 2a). The disassembly buffer for the DisA-TS was then prepared according to the results of this experiment. Reaction analysis was carried out by an SEC-HPLC method, where the mobile phase composition was the same as the examined disassembly reaction conditions. Compared with using a standard analysis mobile phase, the disassembly reaction is less influenced using the mobile phase at disassembly conditions. The selected 300 Å pore size SEC-HPLC column led to separation of VLPs, dimers (capsomeres), and lower-molecular-weight species (LMWS) such as buffer substances, host cell proteins, and nucleic acids while ensuring a short total analysis time of 7.5 min. For a particular disassembly condition, this enabled the analysis of four batches, here two different VLPs in duplicates, with a time interval of 30 min between each sampling.

DisA-OC: For determining initial disassembly rates, the above-mentioned SEC-HPLC method was directly used as a screening tool (Figure 2c). Here, one needs to keep in mind that the reaction conditions are slightly different from the SEC-HPLC analysis in the DisA-TS, due to the unprocessed nature of the sample (pH 7.2, no urea) and the immediate fractionation of the sample composition based on size and structure of the molecules.

3.1 | Disassembly rate

Regarding the DisA-TS results, the slope of the dimer yield between the first measured sample ($t_1 + \Delta\bar{t}_{ret} \approx 33.36$ min) and the starting VLP solution (t_0) can be converted into an approximate initial disassembly rate $k_{0,DisA\text{-}TS}$ (Equation 3). For a better temporal resolution of the initial disassembly rate, the described SEC-HPLC method was used as a screening tool (DisA-OC) reducing the investigated reaction interval to the mean dimer retention time $\Delta\bar{t}_{ret} = 3.36$ min. Here, VLPs in neutral buffer were directly injected into the mobile phase at disassembly conditions, resulting in an on-column disassembly reaction. Figure 3 shows a comparison of the two experimentally determined disassembly rates. While $k_{0,DisA\text{-}OC}$ increased to 4.7 $g{\cdot}L^{-1}{\cdot}h^{-1}$ for Cp149 and to 7.3 $g{\cdot}L^{-1}{\cdot}h^{-1}$ for VLP A, $k_{0,DisA\text{-}TS}$ was 1.1 $g{\cdot}L^{-1}{\cdot}h^{-1}$ at most, confirming that $k_{0,DisA\text{-}OC}$ is a more accurate representation of the initial disassembly rate. Comparing the two screening methods for Cp149, $k_{0,DisA\text{-}OC}$ below 1.0 $g{\cdot}L^{-1}{\cdot}h^{-1}$ resulted in a similar corresponding $k_{0,DisA\text{-}TS}$. This behavior is expected if $k_{0,DisA\text{-}TS}$ is a good representation of the actual initial disassembly rate in the first approximately 33 min. In this study, this is the case if the initial disassembly rate is smaller than 2 $g{\cdot}L^{-1}{\cdot}h^{-1}$ and approximately constant during the observed interval, as the DisA-TS results for Cp149 in Figure 4a suggest. In contrast to Cp149, VLP A showed a steeply increasing dimer yield at the beginning which rapidly flattened out afterward approaching equilibrium (Figure 4), resulting in larger $k_{0,DisA\text{-}OC}$ (Figure 3). For fast disassembly reactions such as for VLP A, $k_{0,DisA\text{-}OC}$ and especially $k_{0,DisA\text{-}TS}$ are determined by dimer concentrations close to the equilibrium. This is why both could potentially serve as a predictive tool to find disassembly-competent VLP candidates or suggest a promising condition range for screening. Here, the experimental effort, resources, and time for a DisA-OC experiment would be significantly lower than for the DisA-TS. For example, the disassembly rates of 96 VLP candidates can be screened for one disassembly condition within 24 h.

3.2 | DisA-TS

The developed DisA-TS was applied to investigate the effect of varying c_{urea}, pH, and the combination of both on HBcAg VLP disassembly. From a process development perspective, a high yield obtained in reasonable process time, including knowledge about a potential operating window, is desirable. It is, therefore, interesting to observe the dimer yield in a time frame of 24 h.

3.2.1 | Urea screening

Figure 4a shows the dimer yield of Cp149 and VLP A at pH 7.2 and varying c_{urea} over time. It has to be noted that the pre-disassembly VLP stock solution also was at pH 7.2 but contained no urea. For

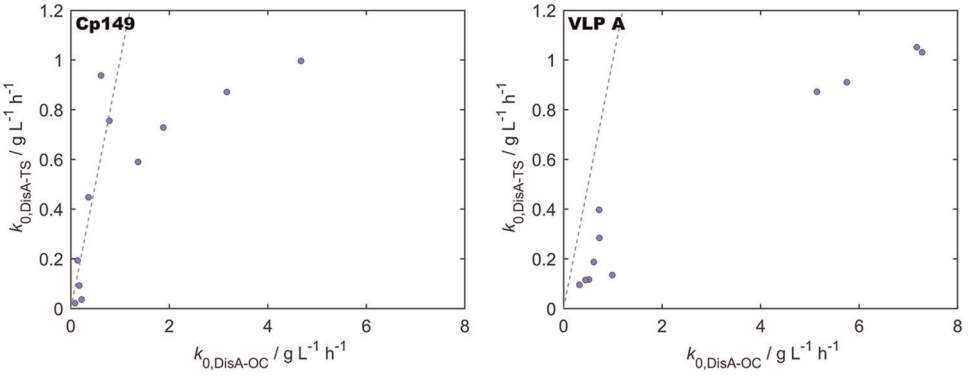

FIGURE 3 Comparison of the disassembly rates from disassembly time series ($k_{0,DisA\text{-}TS}$) and from disassembly on column ($k_{0,DisA\text{-}OC}$) at varying pH and urea concentration. The dashed line indicates equal values of $k_{0,DisA\text{-}TS}$ and $k_{0,DisA\text{-}OC}$. Standard deviations of duplicate measurements are not shown to enhance readability. They were below 0.02 $g{\cdot}L^{-1}{\cdot}h^{-1}$ for $k_{0,DisA\text{-}TS}$ and below 0.18 $g{\cdot}L^{-1}{\cdot}h^{-1}$ for $k_{0,DisA\text{-}OC}$

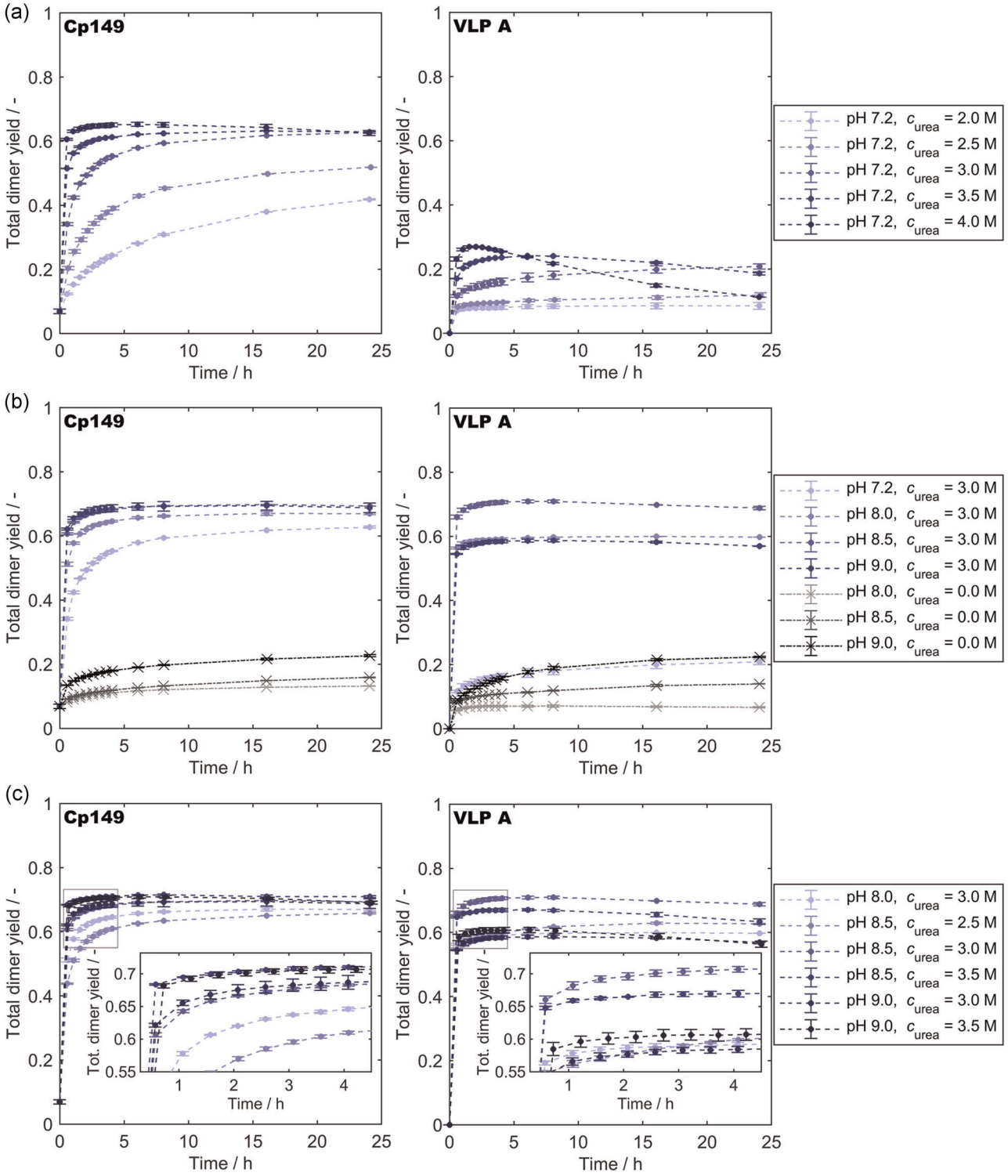

FIGURE 4 Screening of c_{urea} and pH by DisA-TS. Error bars represent the standard deviation of duplicate measurements, and dashed lines were added to guide the eye. (a) DisA-TS of c_{urea} at the same pH as the VLP solution before disassembly, pH 7.2. (b) DisA-TS of pH at a c_{urea} of 3 M (shades of blue) and without urea (shades of black). (c) Combined screening of c_{urea} and pH by DisA-TS. The gray box indicates the position of the magnification shown in the inserted plot. c_{urea}, urea concentration; DisA-TS, disassembly time series; VLP, virus-like particle [Color figure can be viewed at wileyonlinelibrary.com]

Cp149, this condition already resulted in the presence of HBcAg dimers, indicated by an initial dimer yield of 0.07, as similarly observed previously (Singh & Zlotnick, 2003). At the beginning of the reaction ($t \leq 6$ h), the dimer yield increased for all experiments, where a larger c_{urea} led to a stronger increase. After this initial period, the dimer yield still increased for $c_{urea} \leq 3$ M, stagnated for $c_{urea} = 3.5$ M, and decreased for $c_{urea} = 4$ M from a maximum of 0.65 to 0.63. Interestingly, $c_{urea} \geq 3$ M led to a faster yield increase but resulted in a similar final dimer yield of 0.62 at 24 h. VLP A disassembly was at a generally lower level for these conditions. The highest dimer yield after 24 h was observed for $c_{urea} = 3$ M. Similar to Cp149, the dimer yields for a higher c_{urea} increased to a maximum before they declined. This effect was more pronounced for VLP A than for Cp149 and was strongest for $c_{urea} = 4$ M, where the maximum dimer yield of 0.27 was reached after 1.5 h, after which it decreased to 0.11 after 24 h. When dimer aggregation occurs, aggregate species are expected to have a higher molecular weight and therefore elute earlier than dimers in SEC-HPLC. Considering SEC-HPLC chromatograms of these samples (Supporting Information Figure S1), the decline in dimer yield was accompanied by a concentration increase of high-molecular-weight species (HMWS), pointing toward aggregation. This suggests that VLP A is more susceptible to urea-based degradation. VLP A differs from Cp149 by the inclusion of a C-terminal His-tag and the integration of an epitope into the spike tip of the protein. The spike tip insertion could have an impact on dimer stability and thus influence its susceptibility toward urea degradation. The generally higher dimer yield at equal solution conditions for Cp149 as compared with VLP A might also be influenced by the inserted epitope, as an influence of insertions on VLP assembly and stability has been shown (Billaud et al., 2005; Karpenko et al., 2000). Interestingly, it has been reported that the addition of a C-terminal polyhistidine tag leads to stabilized VLP structures that are more resilient toward mechanical and chemical stress (Schumacher et al., 2018). As a chemical stress, disassembly may be hampered by the addition of a C-terminal polyhistidine tag, which could explain the lower dimer yields for VLP A as compared with Cp149 as observed at pH 7.2.

3.2.2 | pH screening

Figure 4b presents data of pH screenings at $c_{urea} = 0$ M and $c_{urea} = 3$ M for Cp149 and VLP A. For both VLPs and c_{urea}, the dimer yield increased until 6 to 8 h. For most experiments, the dimer yield subsequently remained approximately constant. Experiments without urea and a pH ≥8.5 as well as $c_{urea} = 3$ M, pH 7.2 showed a dimer yield increase from 8 to 24 h. For high pH and c_{urea}, a slight decrease in dimer yield was observed. However, this decrease was less pronounced than for the experiments at $c_{urea} = 4$ M, as described above. An interesting observation is that for $c_{urea} = 3$ M, the experiment at pH 9.0, compared with the experiment at pH 8.5, showed slightly lower dimer yields for Cp149 and significantly lower dimer yields for VLP A. This decrease was probably caused by aggregation. This is supported by chromatograms of the pH 9 experiment, showing increased peak areas for HMWS (data not shown). In both experimental series, VLP A dimer yield increased faster relative to its respective maximum dimer yield. As explained above, Cp149 is substantially more inclined to disassemble at pH 7.2 while the experiments at pH >7.2 did not result in a comparable trend, showing a more similar disassembly progress for VLP A and Cp149. Except for mild and aggregate-promoting conditions, dimer yields showed a plateau toward the end of the DisA-TS (24 h), as observed previously (Singh & Zlotnick, 2003).

3.2.3 | Synergistic effects

The combination of increasing pH and c_{urea} generally led to higher dimer yields as compared with pH or c_{urea} increase alone. Figure 4c shows Cp149 and VLP A dimer yield over time for various combinations of high pH (pH 8 to 9) and c_{urea} (2.5 to 3.5 M). A magnification of the figure reveals that for Cp149, high c_{urea} and pH led to a steeper yield increase, which, however, resulted in similar final dimer yields of 0.66 to 0.71 after 24 h. For VLP A, this general trend is not applicable. VLP A showed yield decreases over the time course of the experiments at pH ≥ 8.5, indicating aggregation. Final dimer yields ranged from 0.56 to 0.69, where the highest final yield was observed for pH 8.5 and $c_{urea} = 3$ M. Generally, it has to be noted that dimer yields below 1 are commonly observed for disassembly of *in vivo*-assembled VLPs, for example, 0.58 to 0.89 in a recent publication (Zhang et al., 2021). This behavior is expected for *in vivo*-assembled VLPs, where dis- and reassembly aim to remove inactive protein (Zlotnick et al., 2002).

A comprehensive overview of the impact of reaction conditions on maximum dimer yield and $k_{0,DisA\text{-}OC}$ is given in Figure 5. While $k_{0,DisA\text{-}OC}$ was similar for Cp149 and VLP A at pH 7.2, the maximum dimer yield was significantly higher for Cp149. At higher pH and c_{urea}, dimer yields were comparable between Cp149 and VLP A, while $k_{0,DisA\text{-}OC}$ was generally higher for VLP A. This illustrates that not only the dimer yield but also $k_{0,DisA\text{-}OC}$ is influenced by the molecular structure of the VLP, in this case, the insertion of a foreign epitope and addition of a C-terminal polyhistidine tag for VLP A. In essence, the screening experiments showed that higher pH and c_{urea} lead to higher dimer yields, which is, however, limited by aggregation, especially for VLP A and at pH 9. The highest dimer yields after 24 h were 0.71 for Cp149 and 0.69 for VLP A, achieved at pH 8.5, $c_{urea} = 3.5$ M and pH 8.5, $c_{urea} = 3$ M, respectively.

3.3 | Filtration-based dis- and reassembly

At a 30 mL scale, DF-based disassembly of Cp149 and VLP A was performed, followed by an 18 h overnight hold, a dimer separation step by dead-end filtration, and DF-based VLP reassembly (Figure 1b). In this study, disassembly is achieved by buffer exchange of 6 diafiltration volumes (DV) into the DF disassembly buffer, which

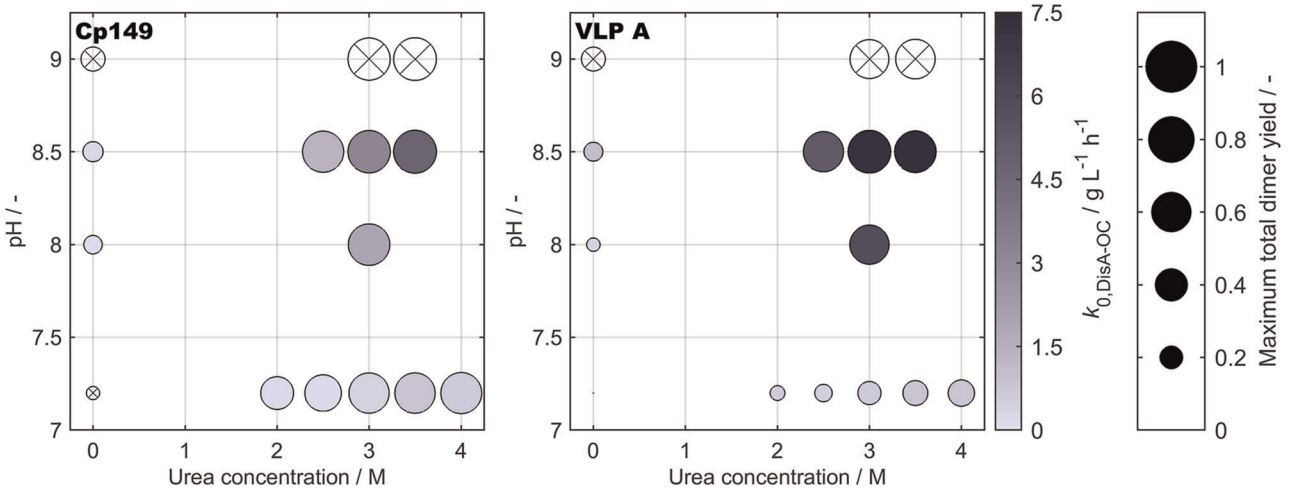

FIGURE 5 Effect of screening conditions on $k_{0,DisA-OC}$ and total dimer yield of Cp149 and VLP A. The center of each bubble determines the screening conditions, urea concentration, and pH. The color intensity and the area of a bubble represent $k_{0,DisA-OC}$ and the maximum of the total dimer yield, respectively. Note that the DisA-OC approach was not performed for conditions at pH 9 due to the pH limit of the SEC-HPLC column. Bubbles of conditions which did not allow for $k_{0,DisA-OC}$ determination are transparent and marked with a black "X." DisA-OC, disassembly on column; HPLC, high-performance liquid chromatography; $k_{0,DisA-OC}$, disassembly rate from disassembly on column; SEC, size-exclusion chromatography [Color figure can be viewed at wileyonlinelibrary.com]

is completed after approximately 90 min considering a permeate flow rate of 2 mL·min^{-1}. An advantage of DF over other disassembly methods is the simultaneous increase in disassembly buffer component concentration and depletion of undesired LMWS (10 kDa MWCO), such as impurities or VLP stability-enhancing salts from previous process steps. This has implications on the design of the DisA-TS and the interested reader is referred to the Supporting Information Section S2. The MWCO selection was based on previous work (Rüdt et al., 2019) and provided full retention of dimers under the conditions used in this study. The conditions for DF-based disassembly were chosen based on the highest dimer yield in the DisA-TS, regardless of disassembly rate $k_{0,DisA-OC}$ (Section 3.1). Considering the expected DF process times and the implementation of an overnight hold, faster disassembly, that is, larger $k_{0,DisA-OC}$, does not result in a significant advantage. Therefore, the disassembly process step was conducted at a target HBcAg concentration of 1 g·L^{-1}, pH 8.5, and $c_{urea} = 3.5$ M for Cp149, or $c_{urea} = 3$ M for VLP A. Another, more differentiated consideration could be the preference of lower pH and urea concentration but a similar dimer yield to prevent "alkaline stress" and to save resources. The results of the DisA-TS revealed that the dimer yield typically continues to increase after 90 min, which is the process time of DF-based disassembly. Therefore, a hold step was implemented after this process step. Another finding of the DisA-TS was that the highest dimer yields are often concomitant with a yield decrease toward the end of the observed 24 h period, especially for VLP A. In pre-experiments for VLP A, the overnight hold at room temperature resulted in a turbid solution that clogged a 0.2 µm pore size filter, indicating aggregation (data not shown). The turbidity of the process solution was avoided by cooling to 5°C during the hold step and was implemented in all presented processes. Another potential measure to prevent aggregation is the supplementation of the disassembly buffer with additives such as NaCl (Singh & Zlotnick, 2003), glycerol (Schumacher et al., 2018), or surfactants (Shi et al., 2005). A screening for additives and their optimal concentration could easily be performed using the developed DisA-TS method, which is, however, out of the scope of this study. As observed in the DisA-TS, the highest dimer yield was 0.71. The remainder of the protein is regarded as inactive protein and is therefore removed in a separation step (Zlotnick et al., 1996, 2002). Here, dead-end filtration with a 0.2 µm syringe filter and a 100 kDa MWCO membrane aimed for removal of undesired species with higher molecular weight than dimers. The MWCO of 100 kDa was selected as it successfully retained VLPs during the preceding purification (Supporting Information Section S1). The permeation of dimers through the centrifugal filter membrane was confirmed by SEC-HPLC in a preliminary test (data not shown). For the subsequent VLP reassembly, DF has proven to be a valuable tool (Liew et al., 2012; Rüdt et al., 2019) and was therefore applied for 3 DV in this study.

3.4 | At-line monitoring of DF-based disassembly

Figure 6 shows the DF-based dimer yield over process time determined by at-line SEC-HPLC. The mobile phase conditions were adapted to the current theoretical buffer composition in the retentate of the CFF unit (Section 2.4) aiming for a minimal bias of the analysis procedure with regard to the measured dimer yield. The same theoretical 280 nm extinction coefficient was used for all mobile phases in this study. It has to be noted that the absorption of proteins at 280 nm increases with increasing urea concentration (Pace et al., 1995) and thereby leads to a relative overestimation of the protein concentration for samples with higher urea

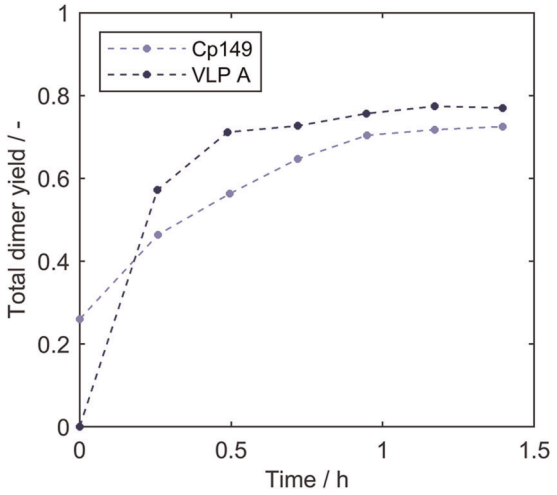

FIGURE 6 Total dimer yield determined by at-line SEC-HPLC during DF-based disassembly. The samples were taken at every DV, and the analysis was completed after a median duration of 13 min. Dashed lines were added to guide the eye. DF, diafiltration; DV, diavolume; HPLC, high-performance liquid chromatography; SEC, size-exclusion chromatography [Color figure can be viewed at wileyonlinelibrary.com]

concentration, which was considered negligible for this study. Compared with DisA-TS, Figure 6 shows a 19%-increased initial (feed) dimer yield for Cp149. The feed solutions were frozen at larger scale than for the DisA-TS, most probably leading to a more pronounced freeze/thaw instability of Cp149 VLPs (Schumacher et al., 2018). The dimer yields at the end of the DF (1.4 h) were 0.73 for Cp149 and 0.77 for VLP A, which are higher compared with the DisA-TS results after 1.6 h with 0.70 and 0.69, respectively. The increased dimer yields for DF-based disassembly may result from the slower change of solution conditions avoiding urea concentration peaks or are due to intensified mixing by CFF.

3.5 | Process data of the filtration-based process sequence

In addition to at-line analysis for dimer quantification during disassembly, all process steps were analyzed by off-line SEC-HPLC using a 1000 Å pore size column. This column allowed for a better separation and quantification of differently sized species as compared with the column used in the disassembly screening. Besides VLPs and dimers, a peak with HMWS larger than VLPs was detected. As already shown in a previous study (Hillebrandt et al., 2020), these HMWS are expected to be forms of HBcAg, such as partially reversible aggregates of VLPs or dimers (Newman et al., 2009; Schumacher et al., 2018), as mainly dimers are detected after disassembly. The recovered mass of each species after each process step is listed in Table 1. Besides the aforementioned species, a shoulder of the dimer peak and LMWS were detected in the 280 nm chromatogram. According to their ultraviolet light spectra, the dimer

TABLE 1 Summary of process data for the filtration-based downstream process

Process step	HMWS mass mg	VLP mass mg	Dimer mass mg	Step yield[a] -	Conc.[a] $g \cdot L^{-1}$	A260/A280[a] -
Cp149						
Feed	**1.17**	**15.89**	**6.93**		0.82	0.61
Disassembly and hold	0	0	**20.04**	0.84	0.67	0.55
Dimer separation	0	0	**16.33**	0.82	0.60	0.55
Reassembly	0.22	**14.19**	1.59	0.87	0.46	0.61
VLP A						
Feed	**10.65**	**13.71**	**0.08**		0.84	0.67
Disassembly and hold	0.20	1.06	**17.76**	0.73	0.62	0.56
Dimer separation	0.11	0.21	**13.91**	0.78	0.51	0.56
Reassembly	0.31	**7.90**	0.87	0.57	0.26	0.63

Note: The product species differ between process steps. HMWS, VLPs, and dimers are regarded as product species of the feed, while dimers are regarded as product species of disassembly and hold and dimer separation. For reassembly, VLPs are regarded as product species. The recovered product species mass of each step is shown in bold. Step yield, concentration, and A260/A280 refer to the product species of each step.

Abbreviations: A260/A280, 260 to 280 nm absorbance peak area ratio; conc., concentration; HMWS, high-molecular-weight species; VLP, virus-like particle.

[a]Refers to the step product species (see "Note").

shoulder is a protein species, which could constitute aggregated or partially unfolded forms (Samandoulgou et al., 2015) of the HBcAg dimers. According to their ultraviolet light spectra, the LMWS are a mixture of nucleic acids, buffer species, and/or proteins (data not shown). The content (by peak area) of LMWS after reassembly was 1.8% for Cp149 and 6.4% for VLP A while the dimer shoulder content was 4.0% and 0%, respectively. As no clear trend was observed, both species were not further investigated.

During the 5°C overnight hold, the Cp149 dimer yield further increased from 0.73 (Figure 6) to 0.84 (Table 1) showing no HMWS or VLPs. A potential reason for the higher dimer yield is the temperature-related pH increase. The strong temperature dependence of the Tris pK_a (Beynon & Easterby, 1996) resulted in a measured increase of ~0.3 pH units for the used DF disassembly buffer. Furthermore, decreasing the temperature might increase the extent of disassembly as the opposite reaction, that is, VLP assembly, is favored at higher temperature (Ceres & Zlotnick, 2002). Due to the cooling costs and the long downtime, the overnight hold seems not profitable at a larger scale and an immediate continuation of the process is suggested in this case. Note, that a potential yield loss due to the 0.2 µm filtration is included in the aforementioned yields and was not separately investigated. For the dimer separation step, the apparent retention coefficient of dimers R_{dimer} was determined under

process conditions. Based on the results in Table 1, R_{dimer} was 0.10 for Cp149 and 0.18 for VLP A. The higher retention of VLP A dimers probably results from the higher level of HMWS. The retained HMWS can build up a fouling layer that has been shown to influence the overall selectivity of a fouled membrane in the case of albumins (Meireles et al., 1991). Another possible explanation could be interaction phenomena resulting from different molecular properties of VLP A compared with Cp149, for example, size, shape, charge, or hydrophobicity. Overall, R_{dimer} describes the real dimer retention under process conditions not solely the ideal dimer retention of the selected membrane. The dimer separation MWCO was not optimized but membranes with a higher MWCO are expected to increase the dimer yield (decrease R_{dimer}) while a lower MWCO might improve the HMWS removal (and vice versa).

The filtration-based process sequence resulted in 14.19 mg of reassembled Cp149 VLPs and 7.90 mg of VLP A, reducing the HMWS content by 0.95 mg (81%) and 10.34 mg (97%), respectively. An interesting observation was that the process with VLP A produced more dimer than VLP was present in the feed solution, indicating that HMWS are, at least partially, disassembly-competent. Product loss during DF-based disassembly, dimer separation, and reassembly was presumably caused by adsorption to the membrane, hold-up volumes, and aggregation. As already observed in the DisA-TS, VLP A showed a greater tendency to aggregate. Next to the disassembly process, aggregation challenges have also been reported for reassembly (Ding et al., 2010; Rüdt et al., 2019). For the interested reader, a detailed interpretation of the VLP A product loss can be found in the Supporting Information Section S3.

The disassembly experiments showed an initial increase of the transmembrane pressure (Supporting Information Figure S2). As this pressure increase is concomitant with the degree of buffer exchange and comparably constant toward the end, it can most probably be attributed to the viscosity increase (van Reis & Zydney, 2010) due to the increasing urea concentration (Kawahara & Tanford, 1966). Reassembly experiments showed slightly decreasing transmembrane pressures over time (Supporting Information Figure S2). Overall, DF-based dis- and reassembly resulted in low mean transmembrane pressures of 0.15 and 0.10 bar, respectively, with mean absolute deviations of 0.01 bar for each run. For both membranes, cleaning according to the manufacturer's instructions recovered the water permeabilities compared with the ones before the experiment (note that new membranes were conditioned during pre-experiments to avoid yield or permeability loss due to adsorptive effects). To this end, membrane fouling had no noticeable effect on the filtration performance and was not irreversible. Nevertheless, the permeate flux and membrane loading (amount of retained solutes per membrane area) were comparably low (Liew et al., 2012; Rosenberg et al., 2009; Rüdt et al., 2019; van Reis et al., 1997) and not optimized in this study. Hence, membrane fouling and product quality should be carefully investigated when these parameters are increased for economic reasons.

The 260 to 280 nm absorbance ratio (A260/A280) is an indicator for the nucleic acid content in a protein solution (Layne, 1957; Porterfield & Zlotnick, 2010) but is also influenced by the solution conditions, such as the urea concentration (Donovan, 1969; Pace et al., 1995). Therefore, only samples analyzed under the same solution conditions can be compared, which are feed and reassembly as well as disassembly/hold and dimer separation. For Cp149, the A260/A280 was equal for these pairs (Table 1). It was 0.61 for the feed and after VLP reassembly, where 0.60 was previously regarded as pure non-truncated HBcAg monomer in water, based on theoretical considerations (Porterfield & Zlotnick, 2010). The A260/A280 of dimers after disassembly was 0.55 for Cp149 and 0.56 for VLP A and remained constant after dimer separation. The Cp149 A260/A280 is comparable to 0.57 obtained by affinity chromatography at a urea concentration of 4 M (Zhang et al., 2021). The A260/A280 of the VLP A feed was 0.67 and was decreased to 0.63 after reassembly, indicating the removal of nucleic acids. It is important to mention that the feed A260/A280 in Table 1 is calculated based on the peak areas of HMWS, VLPs, and dimers while it was 0.64 for the VLP peak, suggesting that the depleted nucleic acids were mainly associated with (or bound to) the HMWS. This was also observed in a recent study with murine polyomavirus VLPs (Gerstweiler et al., 2021). Both VLPs used in this study lack the C-terminal protamine-like region of the wild-type HBcAg, which reduces packaging of nucleic acids (Crowther et al., 1994; Zlotnick et al., 1997). Considering VLPs with a higher nucleic acid burden, the developed process sequence could demonstrate even better separation capacities. For further improvement of the purification performance, strongly bound nucleic acids could be digested by a nuclease after disassembly (Zhang et al., 2021) and nucleotides washed out as described previously (Hillebrandt et al., 2020). Another reason for dis- and reassembly lies in the improvement of particle structure and homogeneity (Mach et al., 2006; Zhao, Allen, et al., 2012). This could be shown, especially for VLP A, by the reduction of the HMWS content, suggesting improved VLP homogeneity.

In summary, the filtration-based process sequence has proven efficient in the realization of dis- and reassembly, depleting impurities, and decreasing the HMWS content. An observation during DF-based reassembly was the presence of a small fraction of unassembled protein at the end of the process. A polishing step by flow-through multimodal SEC (Hillebrandt et al., 2020) or an integrated formulation step by DF are conceivable. The integrated formulation step could simultaneously deplete residual unassembled protein and LMWS by appropriate choice of the MWCO, for example, 300 kDa.

4 | CONCLUSIONS

In this study, we developed a low-volume and high-resolution screening for VLP disassembly conditions. Regarding time and material consumption, this method allows for an efficient determination of the dimer yield and kinetic data of VLPs and is thereby a powerful tool to accelerate VLP downstream process development. Two method variants were developed, one with minimal impact on the

disassembly conditions and therefore resulting in an accurate description of the disassembly reaction. Another variant, DisA-OC, allows for higher throughput serving as an indicator for VLP disassembly efficiency of the tested solutions. A synergistic effect of pH and urea on the dimer yield was shown for both investigated *in vivo*-assembled HBcAg VLPs, whereas differences in disassembly rate and aggregation tendency were observed. In the second part of this study, a filtration-based downstream process for VLPs was developed focusing on DF-based disassembly. Here, the optimized disassembly conditions derived from the high-throughput screening were applied and achieved even higher dimer yields of up to 0.84 and a simultaneous reduction of nucleic acids. In the following process steps, capsomeres (HBcAg dimers) were separated from larger species and successfully reassembled to VLPs proving the feasibility of a solely filtration-based VLP downstream processing. The predominantly size-based separations in this approach promise a simple transfer to other chimeric VLP candidates or VLPs.

ACKNOWLEDGMENTS

This project received funding from Deutsche Forschungsgemeinschaft (DFG) in the frame of SPP 1934, project number 273937032. The authors would like to thank BioNTech Protein Therapeutics (Thorsten Klamp and Anja Wilming) as well as Adam Zlotnick and Kim Young for the provision with VLP production plasmids. The authors express their gratitude to Heidemarie Knierim for proofreading. Open Access funding enabled and organized by Projekt DEAL.

AUTHOR CONTRIBUTIONS

Jürgen Hubbuch initiated and supervised the work. Christina H. Wegner performed pre-experiments that provided substantial knowledge to evolving the concepts of this study. Annabelle Dietrich performed the experiments and prepared the data for analysis. Nils Hillebrandt and Philipp Vormittag evolved the concepts and setup presented in this manuscript, aided in and supervised experimental work, analyzed and interpreted the data, and conceptualized the figures. Nils Hillebrandt drafted the final figures and the final manuscript. Nils Hillebrandt, Philipp Vormittag, Annabelle Dietrich, Christina H. Wegner, and Jürgen Hubbuch read and approved the final manuscript.

DATA AVAILABILITY STATEMENT

The data that support the findings of this study are available from the corresponding author upon reasonable request. The amino acid sequence of VLP A cannot be made available because it is confidential industry data.

NOMENCLATURE

A260/A280	absorbance ratio 260 to 280 nm
CFF	cross-flow filtration
DF	diafiltration
DisA-OC	disassembly on column
DisA-TS	disassembly time series
DV	diafiltration volumes
HBcAg	hepatitis B core antigen
HMWS	high-molecular-weight species
HPLC	high-performance liquid chromatography
LMWS	low-molecular-weight species
MWCO	molecular weight cut-off
SEC	size-exclusion chromatography
VLP	virus-like particle

SYMBOLS

c_i	concentration of component i
$\bar{c}_i$	average concentration of component i
$\tilde{c}_i$	measured concentration of component i
f_v	evaporation correction factor
$k_{0,j}$	disassembly rate, further specified by j
R_i	apparent retention coefficient of component i
r_v	volumetric solvent evaporation rate
t_0	time of the start of the experiment
t, t_j	time after start of the experiment (further specified by $j \neq 0$)
$\overline{t_j}$	average time, further specified by j
V, V_j	volume (further specified by j)
Y_i	yield of component i

ORCID

Nils Hillebrandt http://orcid.org/0000-0002-3097-3140

REFERENCES

Beynon, R. J., & Easterby, J. S. (1996). *Buffer solutions* (1st ed.). Oxford University Press Inc. https://doi.org/10.4324/9780203494691

Billaud, J.-N., Peterson, D., Barr, M., Chen, A., Sallberg, M., Garduno, F., Goldstein, P., McDowell, W., Hughes, J., Jones, J., & Milich, D. (2005). Combinatorial approach to hepadnavirus-like particle vaccine design. *Journal of Virology*, *79*(21), 13656–13666. https://doi.org/10.1128/JVI.79.21.13656

Bin Mohamed Suffian, I. F., Garcia-Maya, M., Brown, P., Bui, T., Nishimura, Y., Palermo, A. R., Ogino, C., Kondo, A., & Al-Jamal, K. T. (2017). Yield optimisation of hepatitis B virus core particles in *E. coli* expression system for drug delivery applications. *Scientific Reports*, *7*(1), 43160. https://doi.org/10.1038/srep43160

Borisova, G., Borschukova, O., Skrastina, D., Dislers, A., Ose, V., Pumpens, P., & Grens, E. (1999). Behavior of a short preS1 epitope on the surface of hepatitis B core particles. *Biological Chemistry*, *380*(3), 315–324. https://doi.org/10.1515/BC.1999.043

Bryan, J. T., Buckland, B., Hammond, J., & Jansen, K. U. (2016). Prevention of cervical cancer: Journey to develop the first human papillomavirus virus-like particle vaccine and the next generation vaccine. *Current Opinion in Chemical Biology*, *32*, 34–47. https://doi.org/10.1016/j.cbpa.2016.03.001

Bull, H. B., Breese, K., Ferguson, G. L., & Swenson, C. A. (1964). The pH of urea solutions. *Archives of Biochemistry and Biophysics*, *104*(2), 297–304. https://doi.org/10.1016/S0003-9861(64)80017-5

Böttcher, B., Vogel, M., Ploss, M., & Nassal, M. (2006). High plasticity of the hepatitis B virus capsid revealed by conformational stress. *Journal of Molecular Biology*, *356*(3), 812–822. https://doi.org/10.1016/j.jmb.2005.11.053

Ceres, P., & Zlotnick, A. (2002). Weak protein–protein interactions are sufficient to drive assembly of hepatitis B virus capsids. *Biochemistry*, *41*(39), 11525–11531. https://doi.org/10.1021/bi0261645

Chackerian, B. (2007). Virus-like particles: Flexible platforms for vaccine development. *Expert Review of Vaccines*, *6*(3), 381–390. https://doi.org/10.1586/14760584.6.3.381

Crowther, R. A., Kiselev, N. A., Böttcher, B., Berriman, J. A., Borisova, G. P., Ose, V., & Pumpens, P. (1994). Three-dimensional structure of hepatitis B virus core particles determined by electron cryomicroscopy. *Cell*, *77*(6), 943–950. https://doi.org/10.1016/0092-8674(94)90142-2

Ding, Y., Chuan, Y. P., He, L., & Middelberg, A. P. J. (2010). Modeling the competition between aggregation and self-assembly during virus-like particle processing. *Biotechnology and Bioengineering*, *107*(3), 550–560. https://doi.org/10.1002/bit.22821

Donovan, J. W. (1969). Ultraviolet absorption. In S. J. Leach (Ed.), *Physical principles and techniques of protein chemistry* (1st ed, pp. 101–170). New York: Academic Press. https://doi.org/10.1016/B978-0-12-440101-3.50009-6

European Medicines Agency. (2015). *European public assessment reports: Mosquirix*. https://www.ema.europa.eu/en/documents/medicine-outside-eu/mosquirix-summary-public_en.pdf

Gasteiger, E., Hoogland, C., Gattiker, A., Duvaud, S., Wilkins, M. R., Appel, R. D., & Bairoch, A. (2005). Protein Identification and analysis tools on the ExPASy server. In J. M. Walker (Ed.), *The proteomics protocols handbook* (pp. 571–607). Humana Press. https://doi.org/10.1385/1-59259-890-0:571

Gerstweiler, L., Bi, J., & Middelberg, A. (2021). Virus-like particle preparation is improved by control over capsomere-DNA interactions during chromatographic purification. *Biotechnology and Bioengineering*, *118*, 1688–1701. https://doi.org/10.1002/bit.27687

Ghorbani, A., Zare, F., Sazegari, S., Afsharifar, A., Eskandari, M. H., & Pormohammad, A. (2020). Development of a novel platform of virus-like particle (VLP)-based vaccine against COVID-19 by exposing epitopes: An immunoinformatics approach. *New Microbes and New Infections*, *38*, 100786. https://doi.org/10.1016/j.nmni.2020.100786

Hillebrandt, N., Vormittag, P., Bluthardt, N., Dietrich, A., & Hubbuch, J. (2020). Integrated process for capture and purification of virus-like particles: Enhancing process performance by cross-flow filtration. *Frontiers in Bioengineering and Biotechnology*, *8*, 8. https://doi.org/10.3389/fbioe.2020.00489

Holmes, K., Shepherd, D. A., Ashcroft, A. E., Whelan, M., Rowlands, D. J., & Stonehouse, N. J. (2015). Assembly pathway of hepatitis B core virus-like particles from genetically fused dimers. *Journal of Biological Chemistry*, *290*(26), 16238–16245. https://doi.org/10.1074/jbc.M114.622035

Jegerlehner, A. (2002). A molecular assembly system that renders antigens of choice highly repetitive for induction of protective B cell responses. *Vaccine*, *20*(25–26), 3104–3112. https://doi.org/10.1016/S0264-410X(02)00266-9

Karpenko, L. I., Ivanisenko, V. A., Pika, I. A., Chikaev, N. A., Eroshkin, A. M., Veremeiko, T. A., & Ilyichev, A. A. (2000). Insertion of foreign epitopes in HBcAg: How to make the chimeric particle assemble. *Amino Acids*, *18*(4), 329–337. https://doi.org/10.1007/s007260070072

Kawahara, K., & Tanford, C. (1966). Viscosity and density of aqueous solutions of urea and guanidine hydrochloride. *Journal of Biological Chemistry*, *241*(13), 3228–3232. https://doi.org/10.1016/S0021-9258(18)96519-1

Kurnik, R. T., Yu, A. W., Blank, G. S., Burton, A. R., Smith, D., Athalye, A. M., & van Reis, R. (1995). Buffer exchange using size exclusion chromatography, countercurrent dialysis, and tangential flow filtration: Models, development, and industrial application. *Biotechnology and Bioengineering*, *45*(2), 149–157. https://doi.org/10.1002/bit.260450209

Layne, E. (1957). Spectrophotometric and turbidimetric methods for measuring proteins. In S. P. Colowick & N. O. Kaplan (Eds.), *Methods in enzymology* (Vol. 3, pp. 447–454). Academic Press. https://doi.org/10.1016/S0076-6879(57)03413-8

Lee, K. W., & Tan, W. S. (2008). Recombinant hepatitis B virus core particles: Association, dissociation and encapsidation of green fluorescent protein. *Journal of Virological Methods*, *151*(2), 172–180. https://doi.org/10.1016/j.jviromet.2008.05.025

Liew, M. W. O., Chuan, Y. P., & Middelberg, A. P. J. (2012). Reactive diafiltration for assembly and formulation of virus-like particles. *Biochemical Engineering Journal*, *68*, 120–128. https://doi.org/10.1016/j.bej.2012.07.009

Mach, H., Volkin, D. B., Troutman, R. D., Wang, B.B., Luo, Z., Jansen, K. U., & Shi, L. (2006). Disassembly and reassembly of yeast-derived recombinant human papillomavirus virus-like particles (HPV VLPs). *Journal of Pharmaceutical Sciences*, *95*(10), 2195–2206. https://doi.org/10.1002/jps.20696

McAleer, W. J., Buynak, E. B., Maigetter, R. Z., Wampler, D. E., Miller, W. J., & Hilleman, M. R. (1984). Human hepatitis B vaccine from recombinant yeast. *Nature*, *307*(5947), 178–180. https://doi.org/10.1038/307178a0

McCarthy, M. P., White, W. I., Palmer-Hill, F., Koenig, S., & Suzich, J. A. (1998). Quantitative disassembly and reassembly of human papillomavirus type 11 virus-like particles in vitro. *Journal of Virology*, *72*(1), 32–41. https://doi.org/10.1128/JVI.72.1.32-41.1998

Meireles, M., Aimar, P., & Sanchez, V. (1991). Effects of protein fouling on the apparent pore size distribution of sieving membranes. *Journal of Membrane Science*, *56*(1), 13–28. https://doi.org/10.1016/0376-7388(91)85013-U

Nassal, M., Skamel, C., Kratz, P. A., Wallich, R., Stehle, T., & Simon, M. (2005). A fusion product of the complete *Borrelia burgdorferi* outer surface protein A (OspA) and the hepatitis B virus capsid protein is highly immunogenic and induces protective immunity similar to that seen with an effective lipidated OspA vaccine formula. *European Journal of Immunology*, *35*(2), 655–665. https://doi.org/10.1002/eji.200425449

Newman, M., Chua, P. K., Tang, F.-M., Su, P.-Y., & Shih, C. (2009). Testing an electrostatic interaction hypothesis of hepatitis B virus capsid stability by using an in vitro capsid disassembly/reassembly system. *Journal of Virology*, *83*(20), 10616–10626. https://doi.org/10.1128/JVI.00749-09

Pace, C. N., Vajdos, F., Fee, L., Grimsley, G., & Gray, T. (1995). How to measure and predict the molar absorption coefficient of a protein. *Protein Science*, *4*(11), 2411–2423. https://doi.org/10.1002/pro.5560041120

Phillips, A. T., & Signs, M. W. (2004). Desalting, concentration, and buffer exchange by dialysis and ultrafiltration. *Current Protocols in Protein Science*, *38*(1), 1–15. https://doi.org/10.1002/0471140864.ps0404s38

Porterfield, J. Z., & Zlotnick, A. (2010). A simple and general method for determining the protein and nucleic acid content of viruses by UV absorbance. *Virology*, *407*(2), 281–288. https://doi.org/10.1016/j.virol.2010.08.015

Pumpens, P., & Grens, E. (2001). HBV core particles as a carrier for B cell/T cell epitopes. *Intervirology*, *44*(2–3), 98–114. https://doi.org/10.1159/000050037

Rosenberg, E., Hepbildikler, S., Kuhne, W., & Winter, G. (2009). Ultrafiltration concentration of monoclonal antibody solutions: Development of an optimized method minimizing aggregation. *Journal of Membrane Science*, *342*(1–2), 50–59. https://doi.org/10.1016/j.memsci.2009.06.028

Rüdt, M., Vormittag, P., Hillebrandt, N., & Hubbuch, J. (2019). Process monitoring of virus-like particle reassembly by diafiltration with UV/Vis spectroscopy and light scattering. *Biotechnology and Bioengineering*, *116*(6), 1366–1379. https://doi.org/10.1002/bit.26935

Samandoulgou, I., Hammami, R., Morales Rayas, R., Fliss, I., & Jean, J. (2015). Stability of secondary and tertiary structures of virus-like particles representing noroviruses: Effects of pH, ionic strength, and temperature and implications for adhesion to surfaces. *Applied and Environmental Microbiology*, *81*(22), 7680–7686. https://doi.org/10.1128/AEM.01278-15

Schumacher, J., Bacic, T., Staritzbichler, R., Daneschdar, M., Klamp, T., Arnold, P., Jägle, S., Türeci, Ö., Markl, J., & Sahin, U. (2018). Enhanced stability of a chimeric hepatitis B core antigen virus-like-particle (HBcAg-VLP) by a C-terminal linker-hexahistidine-peptide. *Journal of Nanobiotechnology*, *16*(1), 39. https://doi.org/10.1186/s12951-018-0363-0

Shi, L., Sanyal, G., Ni, A., Luo, Z., Doshna, S., Wang, B., Graham, T. L., Wang, N., & Volkin, D. B. (2005). Stabilization of human papillomavirus virus-like particles by non-ionic surfactants. *Journal of Pharmaceutical Sciences*, *94*(7), 1538–1551. https://doi.org/10.1002/jps.20377

Singh, S., & Zlotnick, A. (2003). Observed hysteresis of virus capsid disassembly is implicit in kinetic models of assembly. *Journal of Biological Chemistry*, *278*(20), 18249–18255. https://doi.org/10.1074/jbc.M211408200

Strods, A., Ose, V., Bogans, J., Cielens, I., Kalnins, G., Radovica, I., Kazaks, A., Pumpens, P., & Renhofa, R. (2015). Preparation by alkaline treatment and detailed characterisation of empty hepatitis B virus core particles for vaccine and gene therapy applications. *Scientific Reports*, *5*(1), 11639. https://doi.org/10.1038/srep11639

van Reis, R., Goodrich, E. M., Yson, C. L., Frautschy, L. N., Whiteley, R., & Zydney, A. L. (1997). Constant C_{wall} ultrafiltration process control. *Journal of Membrane Science*, *130*(1–2), 123–140. https://doi.org/10.1016/S0376-7388(97)00012-4

van Reis, R., & Zydney, A. L. (2010). Protein ultrafiltration. In M. C. Flickinger (Ed.), *Encyclopedia of industrial biotechnology* (pp. 1–20). John Wiley & Sons, Inc. https://doi.org/10.1002/9780470054581.eib515

Vormittag, P., Klamp, T., & Hubbuch, J. (2020a). Ensembles of hydrophobicity scales as potent classifiers for chimeric virus-like particle solubility—An amino acid sequence-based machine learning approach. *Frontiers in Bioengineering and Biotechnology*, *8*, *395*, 1–15. https://doi.org/10.3389/fbioe.2020.00395

Vormittag, P., Klamp, T., & Hubbuch, J. (2020b). Optimization of a soft ensemble vote classifier for the prediction of chimeric virus-like particle solubility and other biophysical properties. *Frontiers in Bioengineering and Biotechnology*, *8*, 881. https://doi.org/10.3389/fbioe.2020.00881

Yang, Y., Shi, W., Abiona, O. M., Nazzari, A., Olia, A. S., Ou, L., Phung, E., Stephens, T., Tsybovsky, Y., Verardi, R., Wang, S., Werner, A., Yap, C., Ambrozak, D., Bylund, T., Liu, T., Nguyen, R., Wang, L., Zhang, B., … Kwong, P. D. (2021). Newcastle disease virus-like particles displaying prefusion-stabilized SARS-CoV-2 spikes elicit potent neutralizing responses. *Vaccines*, *9*(2), 73. https://doi.org/10.3390/vaccines9020073

Zhang, Y., Liu, Y., Zhang, B., Yin, S., Li, X., Zhao, D., Wang, W., Bi, J., & Su, Z. (2021). In vitro preparation of uniform and nucleic acid free hepatitis B core particles through an optimized disassembly-purification-reassembly process. *Protein Expression and Purification*, *178*, 105747. https://doi.org/10.1016/j.pep.2020.105747

Zhao, Q., Allen, M. J., Wang, Y., Wang, B., Wang, N., Shi, L., & Sitrin, R. D. (2012). Disassembly and reassembly improves morphology and thermal stability of human papillomavirus type 16 virus-like particles. *Nanomedicine: Nanotechnology, Biology, and Medicine*, *8*(7), 1182–1189. https://doi.org/10.1016/j.nano.2012.01.007

Zhao, Q., Modis, Y., High, K., Towne, V., Meng, Y., Wang, Y., Alexandroff, J., Brown, M., Carragher, B., Potter, C. S., Abraham, D., Wohlpart, D., Kosinski, M., Washabaugh, M. W., & Sitrin, R. D. (2012). Disassembly and reassembly of human papillomavirus virus-like particles produces more virion-like antibody reactivity. *Virology Journal*, *9*(1), 52. https://doi.org/10.1186/1743-422X-9-52

Zlotnick, A., Ceres, P., Singh, S., & Johnson, J. M. (2002). A small molecule inhibits and misdirects assembly of hepatitis B virus capsids. *Journal of Virology*, *76*(10), 4848–4854. https://doi.org/10.1128/JVI.76.10.4848-4854.2002

Zlotnick, A., Cheng, N., Conway, J. F., Booy, F. P., Steven, A. C., Stahl, S. J., & Wingfield, P. T. (1996). Dimorphism of hepatitis B virus capsids is strongly influenced by the C-terminus of the capsid protein. *Biochemistry*, *35*(23), 7412–7421. https://doi.org/10.1021/bi9604800

Zlotnick, A., Cheng, N., Stahl, S. J., Conway, J. F., Steven, A. C., & Wingfield, P. T. (1997). Localization of the C terminus of the assembly domain of hepatitis B virus capsid protein: Implications for morphogenesis and organization of encapsidated RNA. *Proceedings of the National Academy of Sciences of the United States of America*, *94*(18), 9556–9561. https://doi.org/10.1073/pnas.94.18.9556

SUPPORTING INFORMATION

Additional Supporting Information may be found online in the supporting information tab for this article.

How to cite this article: Hillebrandt, N., Vormittag, P., Dietrich, A., Wegner, C. H., & Hubbuch, J. (2021). Process development for cross-flow diafiltration-based VLP disassembly: A novel high-throughput screening approach. *Biotechnology and Bioengineering*, 1–15. https://doi.org/10.1002/bit.27868

APPENDIX A

DERIVATION OF THE EVAPORATION CORRECTION FACTORS (EQUATION 2)

The calculation of the evaporation correction factor requires a prior determination of the volumetric solvent evaporation rate

$$r_v = \frac{V(t_v) - V(t_0)}{t_v - t_0}, \tag{A1}$$

where V is the solution volume, t_0 the starting time, and t_v the end of the observed interval. Note that r_v is negative in this case and assumed to be constant over time. Proteins, such as HBcAg, do not evaporate and therefore mass conservation holds

$$V(t_0)\,\bar{c}_{HBcAg}(t_0) = V(t_v)\,\bar{c}_{HBcAg}(t_v), \tag{A2}$$

where $\bar{c}_{HBcAg}$ is the average HBcAg concentration of multiple observations and disassembly conditions. Substituting $V(t_v)$ in Equation (A1) with Equation (A2) leads to a mean evaporation rate

$$r_v = \frac{V(t_0)\left(\frac{\bar{c}_{HBcAg}(t_0)}{\bar{c}_{HBcAg}(t_v)} - 1\right)}{t_v - t_0}. \tag{A3}$$

For the DisA-TS, this previously determined mean evaporation rate is then used to compare the evaporation-corrected sample volume $V_c(t)$ at a time t with a theoretical sample volume $V_{th}(t)$. The latter is solely based on volume reduction by sampling (drawn injections) from the initial volume. The reduced volumes $V_c(t)$ and their relation to the theoretical volumes $V_{th}(t)$ is expressed by evaporation correction factors:

$$f_v(t) = \frac{V_{th}(t)}{V_c(t)} = \frac{V_{th}(t)}{V_{th}(t) + r_v(t - t_0)}, \tag{A4}$$

where $(t - t_0)$ is the current experiment duration. For example, considering an initial volume of 500 µL and a second sample after 60 min (one 20 µL sampling already passed), a theoretical volume of $V_{th} = 500\,\mu L - 20\,\mu L = 480\,\mu L$ is expected when neglecting evaporation. Including an evaporation rate would lead to a smaller corrected volume of $V_c = 480\,\mu L + r_v(t - t_0)$, where $(t - t_0) = 60\,\text{min}$. While in this case, the influence of evaporation is small, it increases for later samples.

Due to volume reduction, the measured dimer concentration $\tilde{c}_{dimer,tot}$ is increased due to mass conservation. The corrected concentration is

$$c_{dimer,tot}(t) = \tilde{c}_{dimer,tot}(t)\frac{(V_{th}(t) + r_v(t - t_0))}{V_{th}(t)}. \quad \text{(A5)}$$

Substituting Equation (A4) into (A5) leads to Equation (2). A potential error of this evaporation correction approach is the neglected influence of differing urea concentrations and pH on evaporation. Furthermore, an increase in urea or buffer species concentration due to evaporation during the DisA-TS was neglected. The maximum urea concentration increase is expected for conditions with $c_{urea} = 4\ M$ at 24 h, which amounts to 0.3 M.